J. Fluid Mech. (1992), *vol.* 235, *pp.* 37–55
Printed in Great Britain

Controlled interactions in a forced axisymmetric jet. Part 1. The distortion of the mean flow

By T. A. LONG AND R. A. PETERSEN†
Department of Aerospace and Mechanical Engineering, University of Arizona, Tucson, AZ 85721, USA

(Received 6 January 1990 and in revised form 7 July 1991)

Controlled resonant interactions between two spinning waves in a turbulent, axisymmetric air jet are documented. Interactions betwen two helical waves with spinning mode numbers of $+m$ and $-m$ induced a $\cos(2m\phi)$ distortion of the mean cross-section. The shape and orientation of the distortion were predictable based on the standing wave pattern. Square and elliptical jets were produced in this way and the spatial distribution of the coherent large-scale motion is documented. The elliptical distortion was comparable in magnitude to a jet issuing from a 2:1 elliptical nozzle. A near-resonance case produced from spinning mode numbers of $m = 0$ and $+2$ was also examined.

1. Introduction

The development of free shear flows is sensitive to boundary conditions. When the large turbulent scales are phase locked due to external excitation it is possible to map their structure and spatial evolution. These coherent structures have been examined in plane mixing layers (Gaster, Kit & Wygnanski 1985), wakes (Wygnanski, Champagne & Marasli 1986), and axisymmetric jets (Strange & Crighton 1985). In each case these coherent structures have been identified as inflexional instabilities of the mean velocity profile (Wygnanski & Petersen 1987).

This observation has led to considerable progress in predicting the spatial structure of large-scale turbulence in the region enveloping the potential core of axisymmetric jets. For example, the spatial evolution of the prevailing frequency of the most energetic turbulence scales can be predicted from eigenvalues calculated from parallel flow, linear stability theory applied to measured mean velocity profiles (Petersen & Samet 1988). When the jet was excited acoustically, radial distributions of phase-averaged velocity could be predicted from the stability eigenfunctions provided the excitation was axisymmetric. Moreover the agreement did not deteriorate as the disturbance amplified in the streamwise direction; excellent agreement between phase-averaged measurement and stability eigenfunctions was observed even when the disturbance had achieved amplitudes as high as 24% of the jet speed (Samet & Petersen 1988). Based on similar measurements it is now apparent that the 'preferred mode' described by Crow & Champagne (1971) is the most amplified shear layer instability at x/D of 4. At every other streamwise location there is a different preferred mode (Petersen & Samet 1988).

If two wavetrains are excited simultaneously quadratic nonlinearities can lead to triad resonances. The conditions for resonant interactions are limited by the dispersion relation for the shear layer. For example, Petersen (1978) demonstrated

† Current address: Jet Propulsion Laboratory, Pasadena, CA 91109, USA.

statistically that the matching of phase speeds between large-scale, coherent structures and subharmonic disturbances was a necessary condition for pairings to occur. This has been verified by Cohen & Wygnanski (1987) using controlled excitations.

The present study is concerned with resonant interactions between two spinning waves and their influence on the jet flow field. Strange (1981) observed large changes in the shape of a jet cross-section when he excited the flow simultaneously with two spinning waves of the same frequency. Excitation with two helical waves spinning in the opposite direction produced jets with elliptical and square cross-sections. Cohen & Wygnanski (1987) later attributed this effect to resonant interactions. Their study, however, was confined to the first diameter downstream from the nozzle. The present study extends those earlier results by following the spatial development of the interaction through the developing region of the jet.

There are several specific objectives. Cohen & Wygnanski were able to produce a resonant interaction between two non-degenerate modes that resulted in a slight distortion of the jet cross-section. It was not clear whether this interaction could be maintained farther downstream where jet curvature was larger. Other investigators (Husain & Hussain 1983; Ho & Gutmark 1987) have studied jets issuing from elliptic nozzles and have observed interesting phenomena such as enhanced entrainment and switching of the principal axes. In those studies the vortex filaments at roll-up had non-uniform curvature and so the phenomena have been attributed mainly to self-induction. In the present case an elliptic jet can be produced from a circular nozzle. Because the boundary conditions are so different between the two types of jet flow it is of interest to know whether some of the same phenomena occur.

Part 1 of this study is concerned with the interaction and spatial evolution of the phase coherent, large-scale turbulence and the influence on the mean flow of the jet. In Part 2 (Petersen & Long 1992) the transfer of energy to broadband turbulence and the control over small-scale turbulence will be considered.

2. Experimental techniques

2.1. *Facilities and measurement procedures*

The experimental facilities used in this investigation are described in detail by Petersen & Samet (1988), and by Long (1988). The studies were confined to the potential core region of a vertical jet of air, 5.08 cm in diameter. The jet speed was 16 m/s which resulted in a Reynolds number of 5×10^4 based on exit conditions. For part of the study the air supply consisted of a compressor and regulator (Long 1988). Later the supply was converted to a centrifugal pump with a speed controller. In either case the jet speed was controlled to within 1 % and the free-stream turbulence level was 0.15 %.

The instrumentation consisted of a ring of eight hot-wire probes equally spaced in polar angle and capable of measuring the streamwise component of velocity. The probe locations are expressed in cylindrical coordinates (x, r, ϕ), where r is the polar radius relative to the jet centreline, ϕ is the polar angle, and x is the streamwise distance from the nozzle exit plane. The hot wires were calibrated *in situ* using plenum pressure as the standard. Hot-wire voltage was digitized and converted to velocity using a calibration polynomial. Calibration error was less than 1 % including drift and data scatter.

A computer-controlled stepper motor was used to simultaneously traverse all eight wires in the radial direction. A cathetometer was used for manual, streamwise

positioning. The radial traverse extended from a radius of 1.0 cm to the radial location where the mean velocity was 10% of the centreline value. Measurement accuracy generally deteriorates with increasing radius because of reverse flow, increasing sensitivity to other components of velocity, and thermal effects.

The jet instabilities were excited acoustically with an array of eight compression drivers located at the nozzle lip and equally spaced in polar angle. A polar array couples most strongly with radial fluctuations. Because of the strong shear close to the nozzle lip this arrangement has proven to be much more efficient in driving streamwise fluctuations than the plenum speaker used in previous experiments (Samet & Petersen 1988).

An acoustic waveguide from each speaker terminated in a rectangular duct. The speakers were driven from a set of digital-to-analogue converters under programme control. The speakers were compensated in amplitude under no-flow conditions using a microphone located on the jet centreline in the nozzle exit plane. Phase shifts introduced by the speakers at the frequencies of excitation were negligible. Because the object was to excite spinning waves the frequencies of excitation were selected to avoid longitudinal acoustic modes of the plenum chamber.

At this point it is appropriate to make a distinction between 'excited' and 'forced' response of the flow. If the amplitude of the imposed disturbance is small then the excited flow instabilities will have small amplitude initially. This will be followed by a region where the instability is linear and the amplitude growth is exponential with streamwise distance. Samet & Petersen (1988) measured amplification ratios as high as 17.1 when the initial disturbance was small. At higher excitation levels the amplification ratio fell to 3.3 and there was considerable broadband distortion of the turbulence spectrum. In the present case, in order to achieve substantial control over the mean flow, the disturbance was introduced at a high enough level that the region of exponential growth was bypassed. In fact there was virtually no amplification of peak values.

It is possible that such differences in initial conditions may have an important impact on the dynamics of the finite-amplitude disturbance that eventually evolves. For that reason some distinction should be made between low-level 'excitation' and stronger 'forcing'.

2.2. *Data processing techniques*

The response of the jet to imposed excitations is documented in terms of the distortion of the mean flow and in terms of spatial distributions of phase-averaged quantities. The basic signal processing techniques are described in this section.

The distortion of the mean flow is expressed in terms of contours of mean velocity in jet cross-sections at various streamwise locations. Radial profiles of mean velocity were measured for each of the eight hot wires using the radial traverse. From each profile, radial locations of specific velocity levels were determined from linear interpolation. Contours of mean velocity were determined as functions of polar angle by fitting the following Fourier series to the radial intercepts:

$$R(\phi) = R_0 + \sum_{m=1}^{4} [a_m \cos(m\phi) + b_m \sin(m\phi)]. \tag{2.1}$$

The coefficients a_m and b_m were determined from the measured radial intercepts R_i according to

$$\begin{Bmatrix} a_m \\ b_m \end{Bmatrix} = \frac{1}{4} \sum_{i=0}^{7} R_i \begin{Bmatrix} \cos(im\pi/4) \\ \sin(im\pi/4) \end{Bmatrix}. \tag{2.2}$$

Following Hussain & Reynolds (1970) streamwise velocity can be decomposed into a time-average component, a phase-averaged fluctuation, and a phase-incoherent fluctuation:

$$u = U + \hat{u} + u', \tag{2.3}$$

where $\hat{u} = \langle u \rangle - U$ and $u' = u - \langle u \rangle$. Phase-averaged velocity $\langle u \rangle$ is defined

$$\langle u(x, r, \phi, t) \rangle = \frac{1}{N} \sum_{n=1}^{N} u(x, r, \phi, t + t_n), \tag{2.4}$$

where the phase reference t_n for the phase-averaged measurements was based on the excitation signal. Slope and level was used as the sampling condition and a latching algorithm was used to prevent multiple triggers in case of noise. The time resolution was $\frac{1}{64}$ of the excitation period and the sample size N was generally about 1000. The standard deviation of the mean was generally less than 0.5%.

Following Gaster *et al.* (1985) a wave travelling on a dispersive, axisymmetric shear layer can be modelled as

$$\hat{u}(x, \eta, \phi, t) = A(x_0) F_u(x, \eta) \exp\left\{ \mathrm{i} \left[\int_{x_0}^{x} \alpha(\xi)\, \mathrm{d}\xi + m\phi - \frac{2\pi n t}{T} \right] \right\} + \text{c.c.}, \tag{2.5}$$

where m is the spinning mode number, n is the harmonic number, T is the period of the forcing signal, α is the streamwise wavenumber component and F_u is the eigenfunction. The dependence on x is caused by shear layer spreading. The cross-stream variation is expressed in terms of the similarity parameter η defined as

$$\eta = \frac{r - R_{0.5}}{\theta}, \tag{2.6}$$

where $R_{0.5}$ is the radius corresponding to $U(r)/U_j = 0.5$, U_j being the jet velocity. The momentum thickness θ is defined as

$$\theta = \int_0^{\infty} \frac{U(r)}{U_j} \left[1 - \frac{U(r)}{U_j} \right] \mathrm{d}r. \tag{2.7}$$

Because the phase-averaged velocity is periodic in t and ϕ it can be decomposed into a Fourier series with coefficients F_{mn}, defined

$$F_{mn}(x, \eta; \phi_0) = \frac{1}{2\pi T} \int_0^{2\pi} \int_0^{T} \langle u(x, \eta, \phi, t) \rangle \exp\left\{ \mathrm{i} \left[m(\phi - \phi_0) - \frac{2\pi n t}{T} \right] \right\} \mathrm{d}\phi\, \mathrm{d}t, \tag{2.8}$$

where ϕ_0 is an arbitrary reference angle. Note that F_{mn} is complex and the modulus $|F_{mn}|$ is the local amplitude of the component with spinning mode number m and harmonic n. It is related to the eigenfunction, F_u, in (2.5) by

$$F_{mn}(x, \eta) = A(x_0) F_u(x, \eta) \exp\left\{ \mathrm{i} \left[\int_{x_0}^{x} \alpha(\xi)\, \mathrm{d}\xi \right] \right\}. \tag{2.9}$$

3. Resonant interactions between degenerate spinning waves

The jet was forced simultaneously with two helical wavetrains spinning in opposite directions. The frequency and streamwise wavenumber components were identical. The azimuthal wavenumber components were equal and opposite. From symmetry the stability eigensolutions are degenerate.

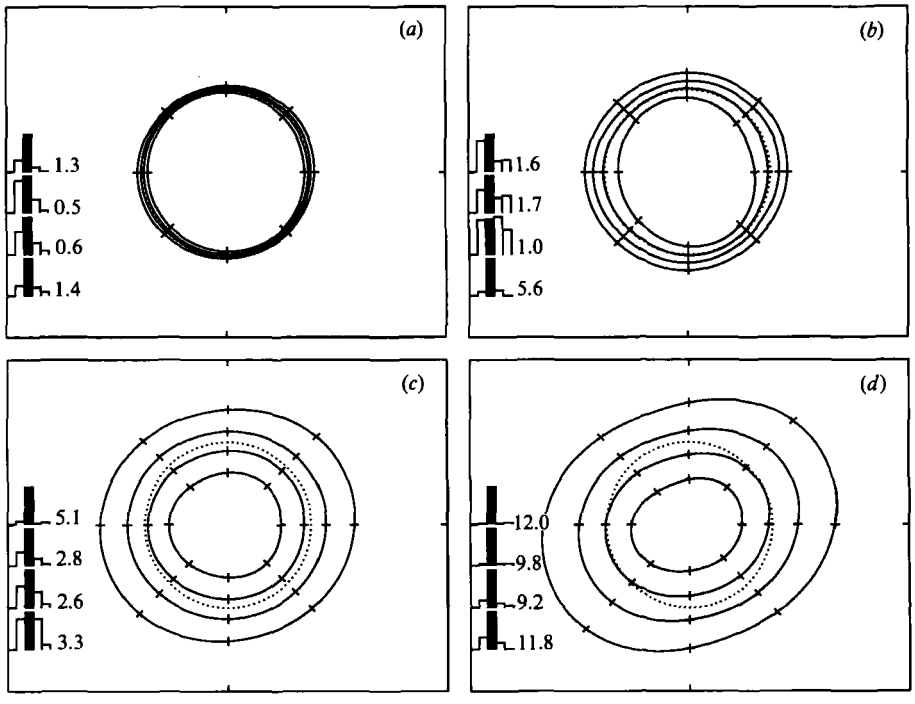

FIGURE 1. Jet cross-section distortion induced by forcing at 206 Hz with spinning mode number combination $m = +1, -1$. Mean velocity contours from $0.3U_j$ to $0.9U_j$ in $0.2U_j$ intervals. Measurement location x/D: (*a*) 0.5; (*b*) 1.0; (*c*) 3.0; (*d*) 4.0.

Assuming that the amplitudes are small, the momentum equation can be modelled by a wave equation driven by a weak nonlinear operator. If the medium is spatially homogeneous and the leading nonlinearity is quadratic then a triad resonance with a third wavetrain is possible provided the three satisfy the following resonance conditions (Phillips 1974):

$$\boldsymbol{k}_1 \pm \boldsymbol{k}_2 \pm \boldsymbol{k}_3 = 0, \tag{3.1}$$

$$\omega_1 \pm \omega_2 \pm \omega_3 = 0, \tag{3.2}$$

where $\boldsymbol{k}$ is the wavenumber vector and ω is the frequency of the wavetrain. The resonance conditions must be compatible with the dispersion relationship in order for a triad resonance to occur.

Cohen & Wygnanski (1987) showed that the following resonance conditions are possible if two unstable wavetrains, denoted by subscripts 1 and 2, travel on an axisymmetric shear layer that is homogeneous in the streamwise direction:

$$\alpha_3 = \alpha_1 - \alpha_2^*; \quad \omega_3 = \omega_1 - \omega_2; \quad m_3 = m_1 - m_2, \tag{3.3}$$

$$\alpha_3 = \alpha_1 + \alpha_2; \quad \omega_3 = \omega_1 + \omega_2; \quad m_3 = m_1 + m_2. \tag{3.4}$$

The subscript 3 denotes the interaction wave and α^* is the complex conjugate of α. The real and imaginary parts of α refer to streamwise wavenumber component and spatial growth rate.

If the two wavetrains are degenerate with spinning mode numbers $+m$ and $-m$, (3.3) leads to an interaction term with frequency and streamwise wavenumber equal to zero (Cohen & Wygnanski 1987):

$$\hat{u}_3 = |F_3(\eta)|\, \mathrm{e}^{-2\alpha_1 x} \cos(2m\phi). \tag{3.5}$$

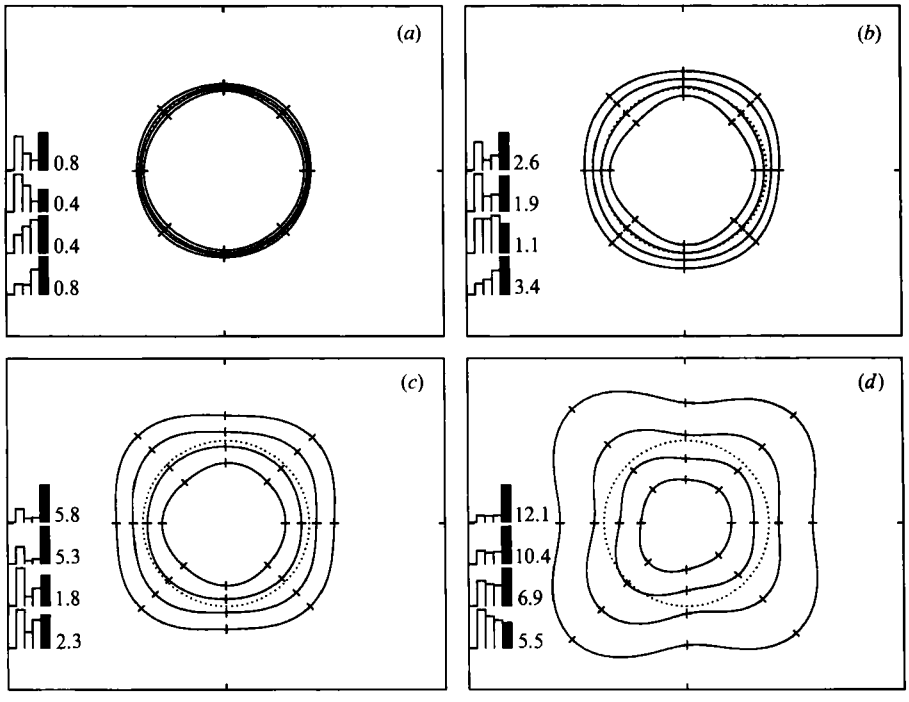

FIGURE 2. Jet cross-section distortion induced by forcing at 206 Hz with spinning mode number combination $m = +2, -2$. Mean velocity contours from $0.3U_j$ to $0.9U_j$ in $0.2U_j$ intervals. Measurement location x/D: (*a*) 0.5; (*b*) 1.0; (*c*) 2.0; (*d*) 4.0.

Physically the superposition of the two wavetrains produces a standing wave pattern. The added mean flow $\hat{u}$ results from the associated wave stresses. The magnitude of the added mean flow grows in the streamwise direction as the product of the two wave amplitudes and causes a $\cos(2m\phi)$ distortion of the jet cross-section.

Spinning wave pairs with mode numbers $m = +1, -1$ and $m = +2, -2$ were produced by the speaker array. The resulting mean flow distortion is shown in figures 1 and 2. Velocity contours determined from the Fourier series (2.1) are shown for jet cross-sections at various streamwise locations. In each case the jet diameter is indicated by the dotted cicle. The modulus $c_m = (a_m^2 + b_m^2)^{\frac{1}{2}}$ of each Fourier coefficient is indicated in the spectral plots. In each cross-section the lowest spectral plot corresponds to the innermost contour. Each spectral plot is normalized by its maximum and c_0, the mean radius, is suppressed. The maximum, expressed as a per cent of c_0, is indicated to the right of each spectrum.

The expected modulation is emphasized by darkening the appropriate spectral coefficient. For the interaction between modes $+1$ and -1, figure 1, the c_2 coefficient corresponding to a $\cos(2\phi)$ distortion, is emphasized. In the case of interaction between modes $+2$ and -2, figure 2, the c_4 coefficient corresponding to a $\cos(4\phi)$ distortion is emphasized. In each case the measured distortion matched the expectation.

Although elliptical and square cross-sections were produced by the forcing, the initial evolution was different from jets produced by elliptical or square nozzles. The shear layer of a jet issuing from a non-circular nozzle rolls up into vortex filaments with generally uniform thickness but with non-uniform curvature (e.g. Ho & Gutmark 1987). Non-uniform curvature leads to strong self-induced distortion of the

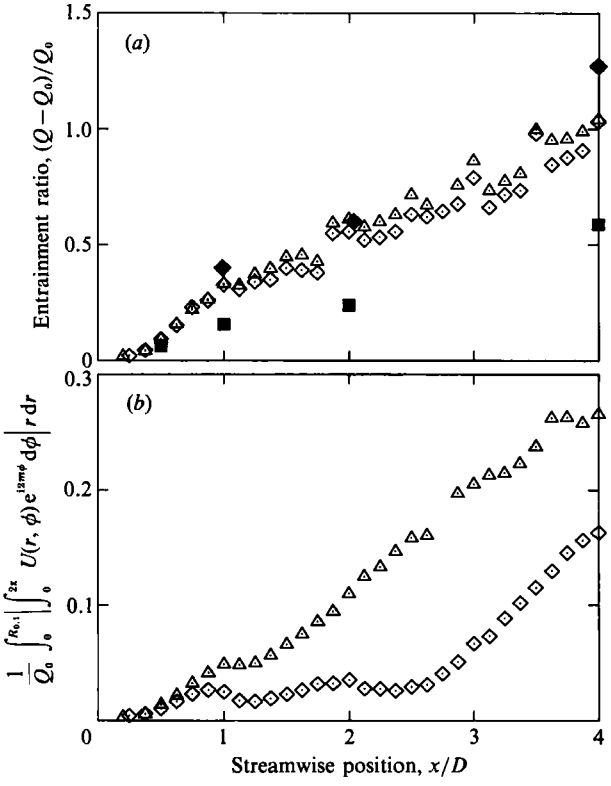

FIGURE 3. Streamwise development of (*a*) entrainment and (*b*) cross-section distortion. Forcing at 206 Hz with spinning mode numbers $+m, -m$: ◇, $m = 1$; △, $m = 2$; ■, no forcing; ◆, 2:1 elliptical nozzle unforced (Ho & Gutmark 1987, figure 17).

filament. In the present case the jet was initially circular and the shear layer was modulated in thickness (figures 1*a* and 2*a*). The uniform distortion of the jet cross-section did not emerge until about $x/D = 2.0$ or 3.0 (figures 1*c* and 2*c*). No axis switching occurred within the potential core region $x/D \leqslant 4.0$.

By the end of the potential core the degree of distortion achieved by forcing spinning mode numbers $m = +1, -1$ was similar to that reported by investigators using 2:1 elliptical nozzles. At $x/D = 4.0$ for example the ratio of the major to minor axes at the half-velocity contour was 1.22 (figure 1*d*) and is identical to the value measured at that location by Husain & Hussain (1983, figure 3, no excitation).

Enhanced entrainment is a more relevant measure because it is a major motivation for the interest in non-circular nozzles. Entrainment ratios, shown in figure 3(*a*), are comparable to those reported by Ho & Gutmark (1987) for a 2:1 elliptical nozzle. It is not clear whether the mechanisms causing the enhanced entrainment are similar. In the present study the added mean flow was the result of wave-induced stresses. It seems unlikely that self-induction of vortex filaments plays an important role in this case. It should be emphasized that the magnitude of enhanced entrainment was the same for spinning mode number combinations $m = +2, -2$ as for $m = +1, -1$. The integrated volume flux Q, truncated at $R_{0.1}$ the radius corresponding to $U/U_j = 0.1$, is defined

$$Q = \int_0^{R_{0.1}} \int_0^{2\pi} U(r,\phi)\, r\, d\phi\, dr. \tag{3.6}$$

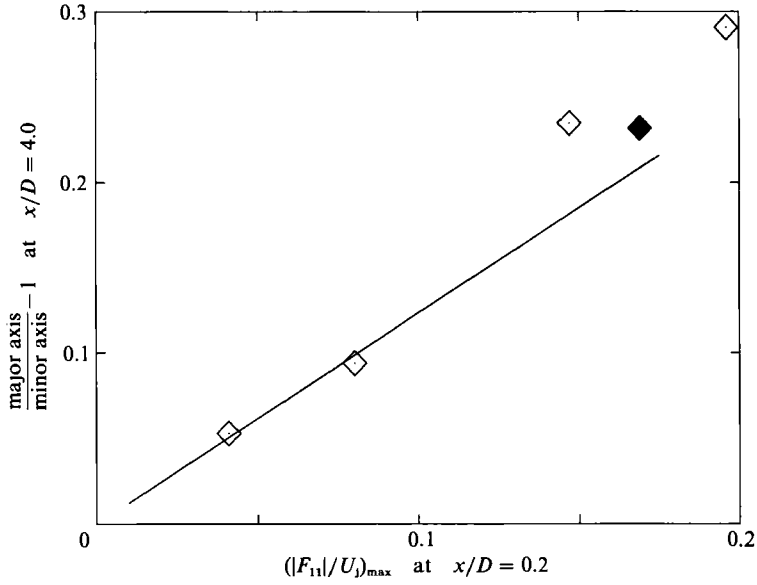

FIGURE 4. Effect of forcing level on mean flow distortion. Forcing at 206 Hz with spinning mode numbers +1, −1. ◆, Forcing level used in this study.

The volume flux was normalized by exit conditions Q_0 defined

$$Q_0 = \tfrac{1}{4}\pi D^2 U_j. \tag{3.7}$$

The eccentricity of the velocity contours varied somewhat from one contour level to the next. Figure 3(*b*) is an integrated measure of eccentricity. Integrals of volume flux have been weighted by $\cos(2m\phi)$. Spinning mode number combinations of $m = +1, -1$ and $m = +2, -2$ are represented by $\cos(2\phi)$ and $\cos(4\phi)$ projections. Initially the magnitudes increased with downstream distance reaching a plateau near $x/D = 1.0$. The plateaux extended to $x/D = 2.5$ in the case of $m = \pm 1$ and to $x/D = 1.3$ in the case of $m = \pm 2$. The plateau regions were bracketed by the cross-sections shown in figures 1 (*b*, *c*) and 2 (*b*, *c*). They mark the transition from modulation of the mixing-layer thickness to distortion of the jet cross-section. Beyond that region the magnitude of the projections increased more or less linearly with x/D.

The resonant interaction and the degree of distortion are functions of the frequency and level of excitation. Their selection was based on a parameter study. The frequency selected was 206 Hz; the corresponding Strouhal number fD/U_j was 0.65. If the frequency was an octave higher, the growth of the disturbance occurred over a much shorter distance and the cumulative effect on the mean flow was weaker. If the frequency was an octave lower the growth was much slower and four diameters was insufficient distance for the mean flow distortion to develop.

The objective in setting the level of forcing was to produce a significant change in the mean flow. In figure 4 the level of cross-section distortion is shown as a function of forcing level in the case of forcing with spinning mode numbers of $m = +1, -1$. The mean flow distortion is expressed in terms of the ratio of major to minor axes of the half-velocity contour measured at $x/D = 4.0$. The forcing level is expressed in terms of the phase-averaged modulus $|F_{11}|_{max}$ measured at $x/D = 0.25$, the measurement station closest to the nozzle exit. Phase-averaged values at that location were proportional to speaker input voltage.

The degree of mean flow distortion at $x/D = 4.0$ increased as the forcing level

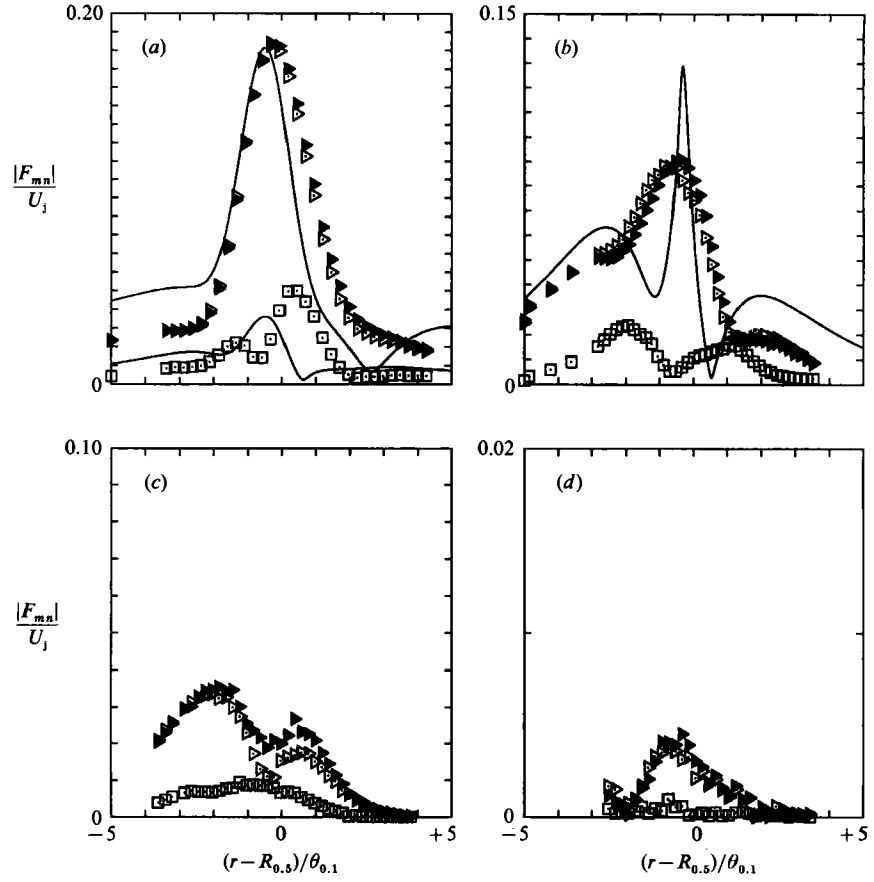

FIGURE 5. Radial profiles of phase-averaged modulus. Forcing at 206 Hz ($n = 1$) and spinning mode numbers $m = +1, -1$. ▷, $m = +1$, $n = 1$; ▶, $m = -1$, $n = 1$; ⊡, $m = 0$, $n = 2$; ——, stability eigenfunctions. (*a*) $x/D = 0.5$, (*b*) 1.0, (*c*) 2.0, (*d*) 4.0.

increased and the trend was roughly linear. The straight line shown in figure 4 was extrapolated from the lowest two data points and is intended to emphasize that the departures from linearity were small. The elliptical distortion shown in figures 1 and 3 was induced using a forcing level corresponding to $|F_{11}|_{\max}/U_j = 0.17$. The same speaker input voltages were used for the spinning mode number combination of $m = +2, -2$.

The measure used in figure 4 to define the forcing level was rather arbitrary. When the forcing is introduced from the plenum it is common to define the forcing level in terms of free-stream fluctuations measured on the centreline in the plane of the nozzle (e.g. Crow & Champagne 1971). When the forcing is introduced from outside the jet as in the present case the disturbance is exponentially damped inside the potential core. Consequently there is some ambiguity in defining the level.

We turn now to the coherent, large-scale motion induced by the forcing. Radial profiles of modulus $|F_{mn}|$, computed according to (2.8), are shown in figures 5 and 6. The momentum thickness $\theta_{0.1}$, based on the measured mean velocity profile and truncated at $R_{0.1}$ (the mean radius corresponding to $U/U_j = 0.1$) is

$$\theta_{0.1} = \int_0^{R_{0.1}} \frac{U(r)}{U_j}\left[1-\frac{U(r)}{U_j}\right]\mathrm{d}r. \tag{3.8}$$

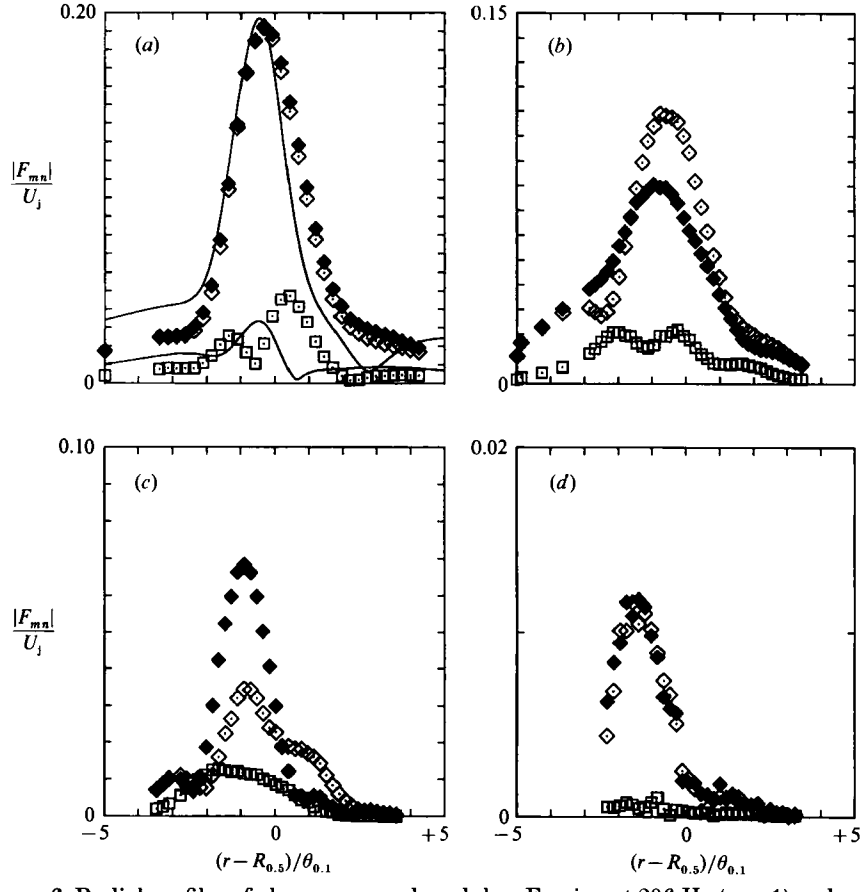

FIGURE 6. Radial profiles of phase-averaged modulus. Forcing at 206 Hz ($n = 1$) and spinning mode numbers $m = +2, -2$. ◇, $m = +2$, $n = 1$; ◆, $m = -2$, $n = 1$; ⊡, $m = 0$, $n = 2$; ——, stability eigenfunctions. (*a*) $x/D = 0.5$, (*b*) 1.0, (*c*) 2.0, (*d*) 4.0.

In each case the frequency of the fundamental $n = 1$ modes was 206 Hz, the forcing frequency. The axisymmetric harmonic ($m = 0, n = 2$) is also shown. The frequency and spinning mode number of this mode correspond to the vector sum of the two forced waves. The wavenumber resonance condition, equation (3.4), will be addressed later. By $x/D = 0.5$ the profile shape of the $m = \pm 1$ mode was identical to the shape of the $m = \pm 2$ mode within measurement resolution. This is consistent with arguments by Cohen & Wygnanski (1987) that stability eigensolutions of low-order spinning modes should be identical in the initial region of the jet. Their argument required both the shear-layer thickness and the streamwise wavelength to be small compared to jet diameter. Those conditions may be too restrictive considering that the wavelength in the present case was approximately one diameter. There was no amplification of peak levels at this high level of forcing. The peak levels decayed monotonically with streamwise distance. We note a departure from symmetry in the radial profiles of degenerate modes $m = +2$ and $m = -2$ in the range $x/D = 1.0$ to 2.0 (figure 6*b*, *c*).

Stability eigenfunctions were calculated at selected locations. They were obtained from inviscid spatial stability theory applied to the measured, mean velocity profile (Petersen & Samet 1988). They were calculated only at locations where the modes

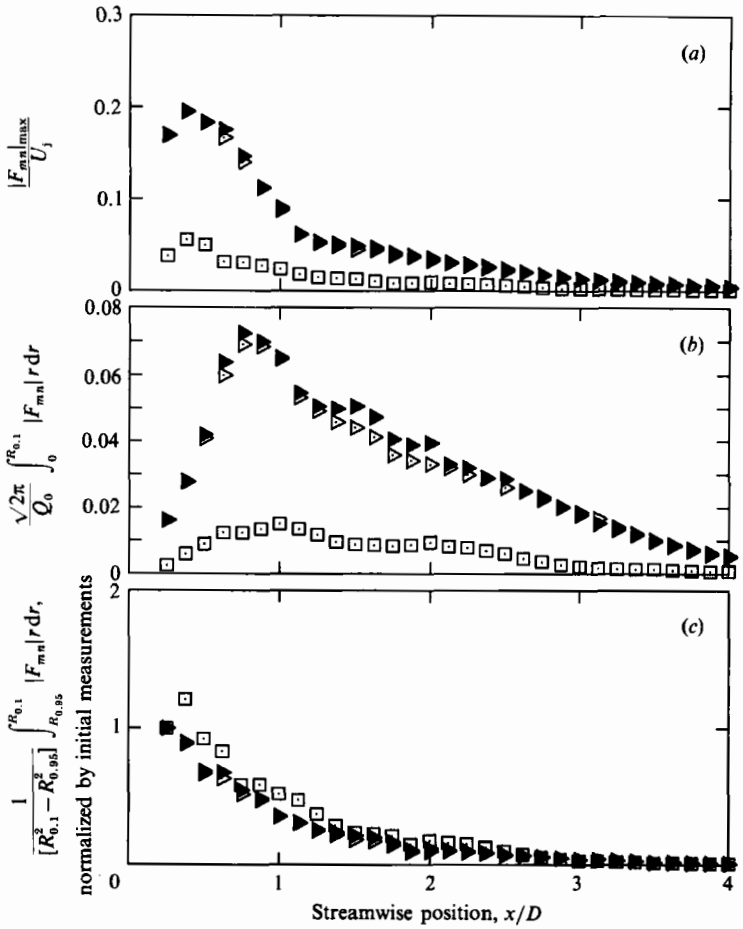

FIGURE 7. Streamwise development of various measures (see text) of coherent, large-scale amplitude. Forcing at 206 Hz ($n = 1$) and spinning mode numbers $m = +1, -1$. ▷, $m = +1$, $n = 1$; ▶, $m = -1$, $n = 1$; ⊡, $m = 0$, $n = 2$.

were linearly unstable. At $x/D = 0.5$ the agreement between measurement and stability theory was reasonably good for the fundamental disturbance. This agreement deteriorated as the mixing-layer thickness increased (e.g. figure 5*b*). Some of this disagreement can be attributed to the distortion of the mean flow. The stability equations assume an axisymmetric base flow. In practice the base flow was modelled after the measured mean profile averaged over polar angle. Asymmetries in the jet cross-section cause spatial smoothing of the phase-averaged measurements and so spatial structure evident in the eigenfunction of figure 5 (*b*) would be difficult to capture experimentally. Possibly the quantitative agreement could be improved by convolving the eigenfunctions with an appropriate spatial filter. The agreement between theory and measurement was poor for the harmonic disturbance at all locations.

The streamwise evolution of the phase-averaged amplitudes is shown in figures 7 and 8. Following the format used by Cohen & Wygnanski (1987) three different measures are presented: (*a*) the maximum amplitude from each radial distribution normalized by the jet speed; (*b*) the amplitude integrated over the cross-section area of the jet and normalized by the exit-plane mass flux $Q_0 = U_j A_0$; and (*c*) the

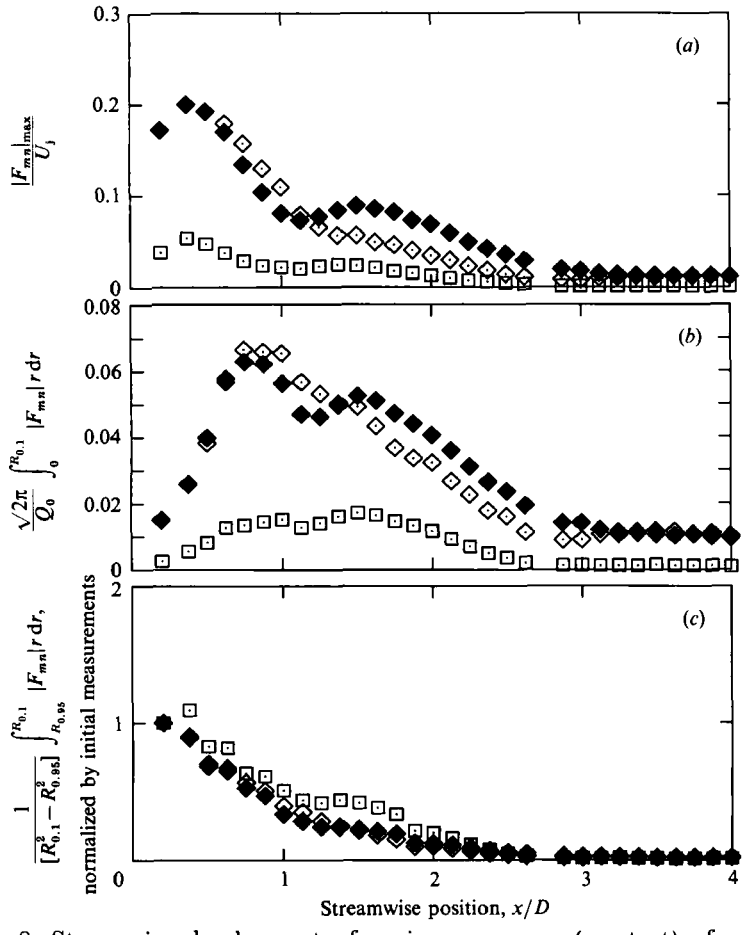

FIGURE 8. Streamwise development of various measures (see text) of coherent, large-scale amplitude. Forcing at 206 Hz ($n = 1$) and spinning mode numbers $m = +2, -2$. ◇, $m = +2$, $n = 1$; ◆, $m = -2$, $n = 1$; ⊡, $m = 0$, $n = 2$.

amplitude averaged over the cross-section and normalized to unity at the initial measurement location. The radial positions $R_{0.95}$ and $R_{0.10}$ correspond to radii where the mean velocities, averaged over time and polar angle, are $0.95U_j$ and $0.10U_j$ respectively. Measure (*a*) is influenced by changes in the shape of the radial profile. Measure (*b*) is strongly influenced by the streamwise spreading of the shear-layer thickness. Measure (*c*) is an attempt to express the growth as an amplification ratio and to eliminate the purely geometric influence of spreading. In computing measure (*b*) the amplitude was divided by $\sqrt{2}$, appropriate to an integrated r.m.s. level of a purely sinusoidal disturbance.

At these high forcing levels there was very little growth evident in either measure (*a*) or (*c*). By contrast Samet & Petersen (1988) measured amplitude gains ranging from 3.3 to 17.1 as the level of excitation was reduced by a factor of 130. Apparently the regime of linear amplification was bypassed in the present case. The growth in integrated amplitude, measure (*b*), was the result of the competition between the spreading of the jet cross-section and the decay of the forced disturbance. The asymmetry between degenerate mode numbers $m = +2$ and -2, evident earlier in figures 6(*b*) and 6(*c*), can be observed also in figure 8. The asymmetry was confined

within the region from $x/D = 1.0$ to 3.0. This region encompasses the transition from $\cos(4\phi)$ modulation of the mixing-layer thickness to $\cos(4\phi)$ distortion of the jet cross-section.

The question of resonance will be considered next. From the standpoint of linear stability theory applied to a parallel base flow, the eigenmodes are degenerate for two waves of the same frequency and opposite spinning mode numbers. In that case resonance condition (3.3) would be satisfied identically. Eigenfunction degeneracy was tested experimentally in figures 5 and 6. Deviations were observed between profiles for $+2$ and -2 spinning mode numbers. This raises questions about the degeneracy of the eigenvalues as well.

The resonance conditions are tested directly by comparing the phase advance of 'resonant' waves. The phase of $F_{mn}(x,\eta)$, equation (2.8), is the delay between the phase-averaged wave and the reference signal. From (2.8) and (2.9) the phase advance can be written

$$\Psi_{mn}(x,\eta) = \psi_{mn}(x_0,\eta) + \int_{x_0}^{x} \alpha_{mn}(\xi,\eta)\,\mathrm{d}\xi. \tag{3.9}$$

The subscripts m and n refer to spinning mode number and harmonic number; $\psi_{mn}(x_0,\eta)$ is the initial phase offset.

As long as the eigenvalues are degenerate the phase difference between two forced waves with opposite spinning mode numbers of $+m$ and $-m$ should be

$$\Psi_{+m1}(x,\eta) - \Psi_{-m1}(x,\eta) = \psi_{+m1} - \psi_{-m1}, \tag{3.10}$$

which is constant along lines of constant η.

Measured phase advances are shown in figure 9. The measurements were made along a ray making an angle of $-7°$ with the nozzle lip. This corresponds roughly to the inner edge of the axisymmetric mixing layer. As expected the phase difference was constant with streamwise distance for both the $m = \pm 1$ and $m = \pm 2$ forcing.

The phase advance of the forced wave alone is included in figure 9 for reference. In both cases the initial wavelength λ/D of the forced wave was about 1. The initial phase speed of the wave with spinning mode number $m = 1$ was approximately 7% greater than the wave with spinning mode number $m = 2$.

Resonance condition (3.4) is also considered in figure 9. The interaction wave corresponding to the vector sum of the two forced waves would have spinning mode number $m = 0$ and harmonic number $n = 2$. Profiles of this mode were included in figures 5 and 6. Along paths of constant η the phase difference between the forced, vector sum and the interaction wave can be written

$$\Psi_{+m1}(x) + \Psi_{-m1}(x) - \Psi_{02}(x) = \int_{x_0}^{x} [2\alpha_{m1}(\xi) - \alpha_{02}(\xi)]\,\mathrm{d}\xi + \text{constant}. \tag{3.11}$$

For resonance the phase difference (3.11) should be uniform with x.

Based on figure 9 the interaction does appear to be resonant beyond $x/D = 1$. initially however the phase difference (3.11) advanced with streamwise distance. The positive slope implies $2\alpha_{m1} > \alpha_{02}$. Consequently the phase speed of the harmonic $2\omega_0/\alpha_{02}$ initially exceeded that of the forced fundamental ω_0/α_{m1}. The origin of the interaction wave is easy to imagine. Distortion either in the speaker output or in the shear-layer response would create harmonics, and imperfect wave cancellation caused either by imperfect speaker compensation or by mean flow distortion would create an axisymmetric component. The initial non-resonance does raise questions

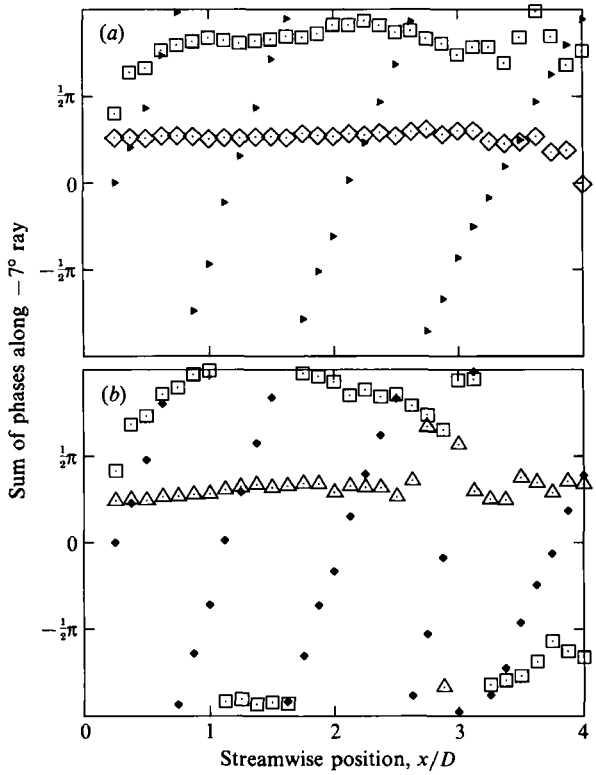

FIGURE 9. Streamwise advance of phase difference along a $-7°$ ray. Phase difference: ◇, $\Psi_{+11}-\Psi_{-11}$; △, $\Psi_{+21}-\Psi_{-21}$; ⊡, $\Psi_{+m1}+\Psi_{-m1}-\Psi_{02}$. Phase advance: ▶, Ψ_{+11}; ◆, Ψ_{+21}. Forced spinning mode numbers: (*a*) $m=+1,-1$; (*b*) $m=+2,-2$.

though about the dynamic significance of the triad resonance. The forced wave stresses were strongest in the first wavelength where the interaction was non-resonant. Based on the distributions shown in figures 7 and 8 there does not seem to be much energy transfer to the harmonic beyond $x/D = 1.0$. However the opportunity for resonant exchange of energy may play a role in the asymmetries observed in figures 6 and 8.

Resonance was indicated in figure 9 by constant phase difference. The value of the constant was determined by the phase offset introduced by the speakers. The spinning waves were introduced with a phase offset to avoid total cancellations in the standing wave pattern at any particular speaker. The effect of varying the phase offset was to change the polar orientation of the mean flow distortion. This occurred in a controlled and predictable manner.

The superposition of two spinning waves propagating along a non-dispersive mixing layer can be modelled as follows:

$$u = \tfrac{1}{2}F_u\, e^{i(\alpha x+m\phi-\omega t-\psi_0)} + \tfrac{1}{2}F_u\, e^{i(\alpha x-m\phi-\omega t)} + \text{c.c.}, \tag{3.12}$$

where ψ_0 is the phase offset. The longitudinal wave stress is

$$\overline{u^2} = |F_u^2|\{1+\cos[2m(\phi-\psi_0/2m)]\}. \tag{3.13}$$

The phase offset should result in a shift in the principal axis by the amount $\psi_0/2m$. This prediction is verified in figure 10 in connection with forced spinning mode

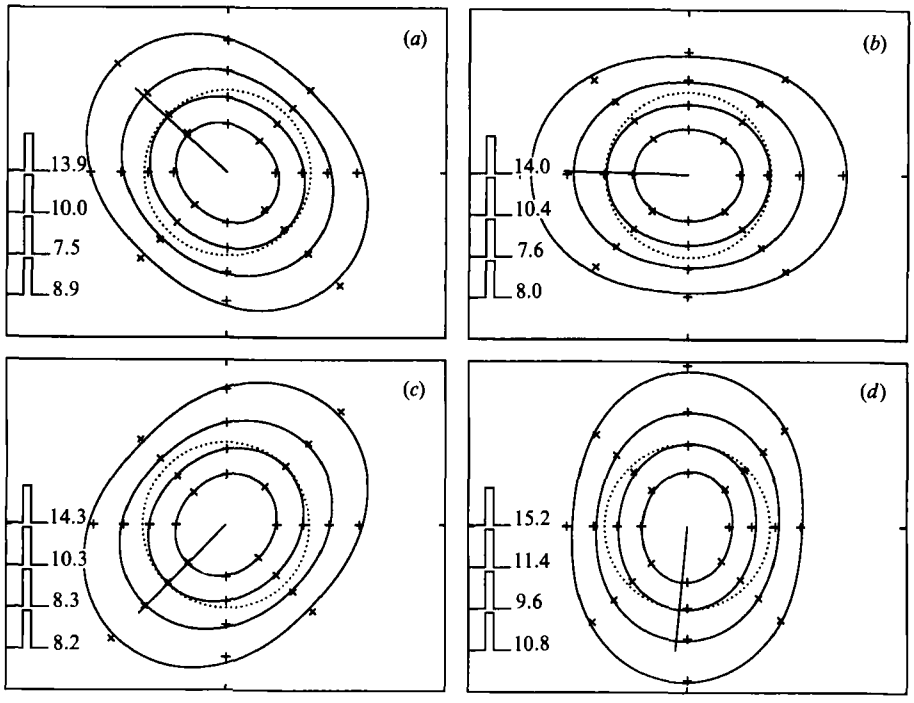

FIGURE 10. Effect of phase offset on jet cross-section at $x/D = 4.0$. Mean velocity contours from $0.3U_j$ to $0.9U_j$ in $0.2U_j$ intervals. Relative phase offset between waves with spinning mode numbers $m = +1, -1$; (*a*) 0°; (*b*) 90°; (*c*) 180°; (*d*) 270°.

numbers $m = +1, -1$. The offset ψ_0 was incremented in steps of $\frac{1}{2}\pi$ and the principal axis advanced in steps of $\frac{1}{4}\pi$ as predicted. For each contour level the polar angle of the principal axis was computed from

$$\phi_0 = \arctan(b_2/a_2). \tag{3.14}$$

The coefficients a_2 and b_2 are Fourier coefficients computed according to (2.2). The principal axes indicated in figure 10 were based on ϕ_0 and averaged over the four contour levels.

4. An interaction between non-degenerate spinning waves

The mean flow distortion of the previous section was the result of resonant interactions between forced waves having equal but opposite spinning mode numbers. Owing to symmetry, the resonance conditions (3.3) were satisfied identically. Under more general conditions the forced interactions may be resonant over limited regions of the flow.

The particular experiment considered here involved forced waves of the same frequency and with spinning mode numbers $m = 0$ and $m = 2$. Based on linear stability theory these modes would be expected to obey the same dispersion relationship in the initial region of the jet. In that case one would expect the resonance conditions (3.3) to induce a $\cos(2\phi)$ modulation of the mean flow. Farther downstream, based on linear stability theory, one would expect the phase speeds of the two modes to diverge.

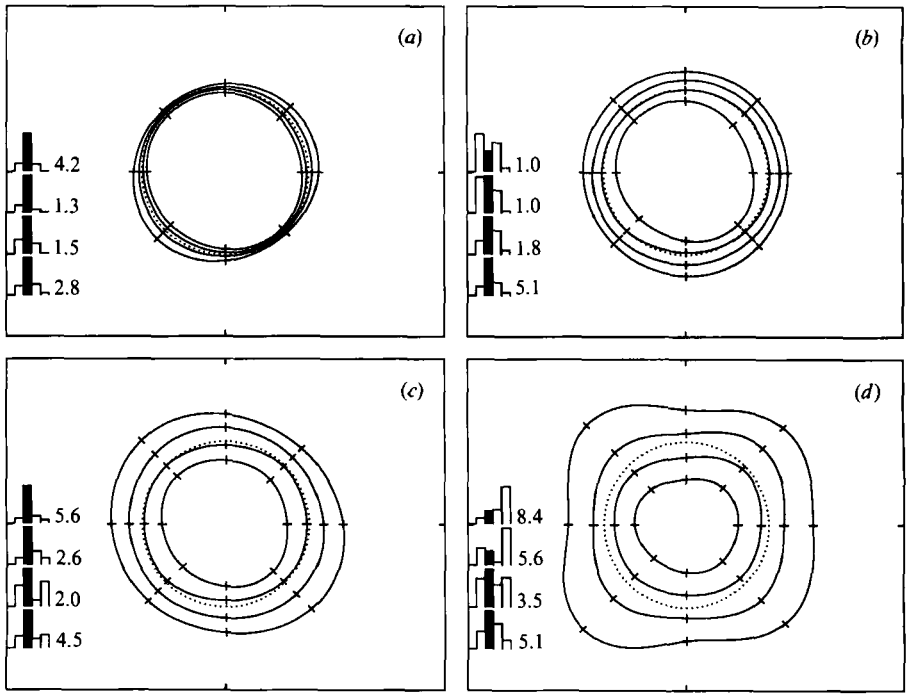

FIGURE 11. Jet cross-section distortion induced by forcing at 206 Hz with spinning mode number combination $m = 0, +2$. Mean velocity contours from $0.3U_j$ to $0.9U_j$ in $0.2U_j$ intervals. Measurement location x/D: (*a*) 0.5; (*b*) 1.0; (*c*) 2.0; (*d*) 3.0.

The evolution of the jet cross-section is shown in figure 11. As predicted the dominant modulation was initially $\cos(2\phi)$ (figure 11*a*, *b*). Beyond $x/D = 2.0$, however, $\cos(4\phi)$ emerged as the dominant cross-section distortion (figure 11*c*, *d*). This was an unexpected result and it resembles the interaction observed earlier (figure 2) in connection with forced waves having a spinning mode number combination of $m = +2, -2$.

Radial profiles of phase-averaged modulus $|F_{m1}|$ are shown in figure 12. The forced modes are shown along with a spurious wave *not deliberately introduced by the speakers* with a spinning mode number of $m = -2$. At $x/D = 0.20$, the measurement station closest to the nozzle lip, the spurious mode was 14% of the $m = 2$ mode. By $x/D = 2.0$ the spurious mode had grown to attain a maximum amplitude 63% of the forced, $m = 2$ mode. Such spurious modes are a feature of helical forcing and they occur even when a single helical wave is forced (Petersen, Samet & Long 1987).

The profile shape of the $m = -2$ mode seems to be a combination of the $m = 0$ and $m = 2$ mode shapes (figure 12*b*). This is indirect evidence that the mode was caused by nonlinearities. Even if the $m = -2$ mode was introduced inadvertently through imperfect compensation between speakers its spatial evolution cannot be explained by simple superposition of linear instabilities.

The streamwise evolution of modulus integrated over the jet cross-section is shown in figure 13. There is evidence of energy exchange from the forced, $m = +2$ mode to the spurious, $m = -2$ mode. Between $x/D = 1.0$ and 2.0 there was a drastic decay in the $m = +2$ mode as compared to the $m = 0$ mode. Beyond x/D of 2.0 the $m = +2$ and $m = -2$ modes seem to track each other and it was in this region of the flow that $\cos(4\phi)$ modulation emerged as the dominant cross-section distortion.

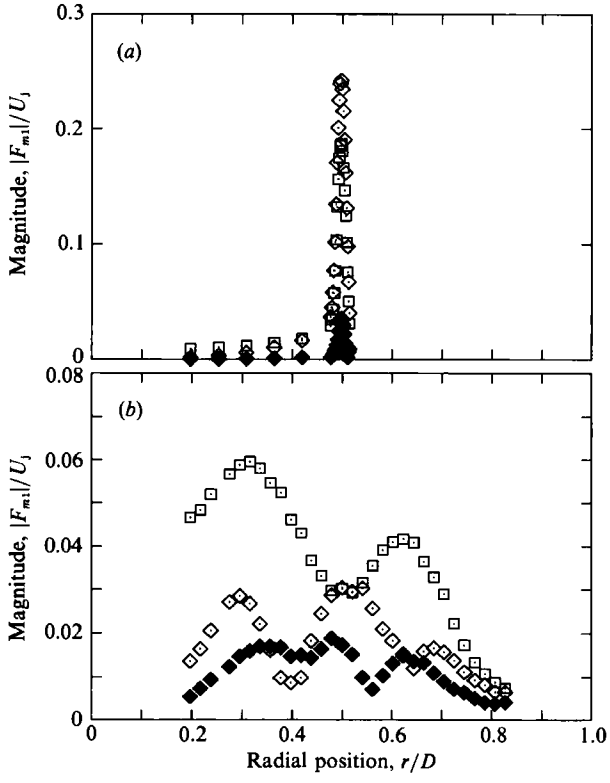

FIGURE 12. Radial profiles of phase-averaged modulus. Forcing at 206 Hz and spinning mode numbers $m = 0, +2$. Spinning mode number: ⊡, $m = 0$; ◇, $m = +2$; ◆, $m = -2$ (spurious mode). (*a*) $x/D = 0.2$, (*b*) 2.0.

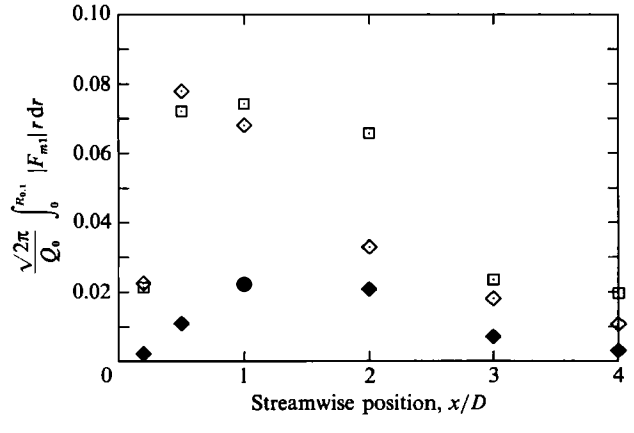

FIGURE 13. Streamwise development of phase-averaged modulus integrated over the jet cross-section. Forcing at 206 Hz and spinning mode numbers $m = 0, +2$. Spinning mode number: ⊡, $m = 0$; ◇, $m = +2$; ◆, $m = -2$ (spurious mode).

Possible resonant interactions of type (3.3) between spinning mode number combinations of $m = 0, 2$ and $m = +2, -2$ are considered in figure 14. Based on the advance of phase difference there are no clear resonances. The slopes of the phase advances imply that the axisymmetric wave travelled faster than either helical wave. The helical wave with spinning mode number $m = +2$ travelled faster than the

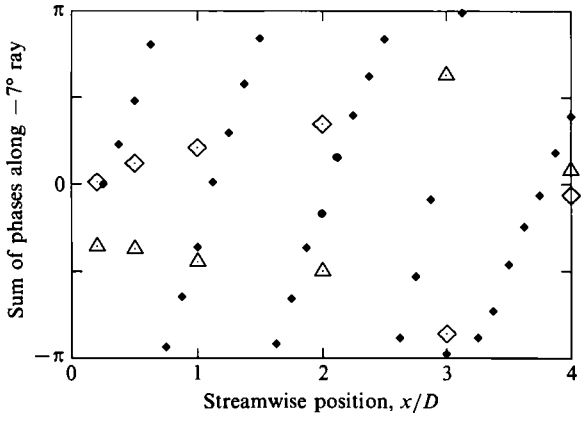

FIGURE 14. Streamwise advance of phase difference along a $-7°$ ray. Forcing at 206 Hz and spinning mode numbers $m = 0, +2$. Phase difference: ◇, $\Psi_{+21} - \Psi_{01}$; △, $\Psi_{+21} - \Psi_{-21}$. Phase advance: ◆, Ψ_{+21}.

wave with mode number $m = -2$. The latter combination was much closer to resonance, though.

5. Conclusions

Two helical waves with the same frequency and with spinning mode numbers of $m = +1$ and $m = -1$ were forced simultaneously and the spatial evolution of their interaction was mapped throughout the potential core region of a jet issuing from a circular nozzle. Similarly the forced interaction between spinning modes of $m = +2$ and $m = -2$ was mapped. As originally reported by Strange (1981) the shape of the jet was drastically altered. Although an attempt was made to optimize the frequency and level of forcing the interactions selected were only two of many possible interactions.

Based on the polar modulation of turbulent stresses caused by the standing wave pattern produced by the interaction between the $m = \pm 1$ modes, a $\cos(2\phi)$ distortion of the mean cross-section was predicted. This was confirmed by direct measurement. The interaction between waves with spinning mode numbers of $m = \pm 2$ produced a $\cos(4\phi)$ distortion of the jet cross-section as predicted. The spatial orientation of the cross-section distortion could be controlled in a predictable way by adjusting the phase offset between the forced waves.

The entrainment ratio was about 1.8 times that of an unforced jet. The enhanced entrainment was comparable to that produced by a 2:1 elliptical nozzle. In contrast to jets issuing from an elliptical nozzle, no vortex curvature effects were observed.

The resonance between forced waves with spinning mode numbers of 0 and $+2$ should produce a $\cos(2\phi)$ distortion of the jet cross-section. While this was initially observed near the nozzle exit, farther downstream the dominant distortion was $\cos(4\phi)$. This unexpected result was produced by the interaction between the forced $m = +2$ mode and a spurious $m = -2$ mode. The spurious mode absorbed energy from the forced mode until the two attained the same order of magnitude.

The authors would like to thank Professor I. Wygnanski for his technical advice. This research was supported by the National Science Foundation under grant MSM 8800086.

REFERENCES

COHEN, J. & WYGNANSKI, I. 1987 The evolution of instabilities in the axisymmetric jet. *J. Fluid Mech.* **176**, 191–235.

CROW, S. C. & CHAMPAGNE, F. H. 1971 Orderly structure in jet turbulence. *J. Fluid Mech.* **48**, 547–591.

GASTER, M., KIT, E. & WYGNANSKI, I. J. 1985 Large-scale structures in a forced turbulent mixing layer. *J. Fluid Mech.* **150**, 23–39.

HO, C. M. & GUTMARK, E. 1987 Vortex induction and mass entrainment in a small-aspect-ratio elliptic jet. *J. Fluid Mech.* **179**, 383–405.

HUSAIN, H. S. & HUSSAIN, A. K. M. F. 1983 Controlled excitation of elliptic jets. *Phys. Fluids* **26**, 2763–2766.

HUSSAIN, A. K. M. F. & REYNOLDS, W. C. 1970 The mechanics of an organized wave in turbulent shear flow. *J. Fluid Mech.* **41**, 241–258.

LONG, T. A. 1988 The controlled interaction of excited modes in an axisymmetric jet. M.S. dissertation, University of Arizona, Tucson.

PETERSEN, R. A. 1978 Influence of wave dispersion on vortex pairing in a jet. *J. Fluid Mech.* **89**, 469–495.

PETERSEN, R. A. & LONG, T. A. 1992 Controlled interactions in a forced axisymmetric jet. Part 2. The modulation of broadband turbulence. *J. Fluid Mech.* **235**, 57–71.

PETERSEN, R. A. & SAMET, M. M. 1988 On the preferred mode of jet instability. *J. Fluid Mech.* **194**, 153–173.

PETERSEN, R. A., SAMET, M. M. & LONG, T. A. 1987 Excitation of azimuthal modes in an axisymmetric jet. In *IUTAM Symp. on Turbulence Management and Relaminarization, Bangalore, India.*

PHILLIPS, O. M. 1974 Wave interactions. In *Nonlinear Waves* (ed. S. Leibovich & A. R. Seebass), pp. 186–211. Cornell University Press.

SAMET, M. M. & PETERSEN, R. A. 1988 Effects of excitation level on the stability of an axisymmetric mixing layer. *Phys. Fluids* **31**, 3246–3252.

STRANGE, P. J. R. 1981 Spinning modes in orderly jet structure and jet noise. Ph.D. dissertation, University of Leeds.

STRANGE, P. J. R. & CRIGHTON, D. G. 1985 Spinning modes on axisymmetric jets. Part 1. *J. Fluid Mech.* **134**, 231–245.

WYGNANSKI, I. J., CHAMPAGNE, F. H. & MARASLI, B. 1986 On the large-scale structures in two-dimensional, small-deficit, turbulent wakes. *J. Fluid Mech.* **168**, 31–71.

WYGNANSKI, I. & PETERSEN, R. A. 1987 Coherent motion in excited free shear flows. *AIAA J.* **25**, 201–213.